Original Research Article: full paper

(2022), «EUREKA: Physics and Engineering»
Number 2

# DEVELOPMENT OF EMPIRICAL MODE DECOMPOSITION BASED NEURAL NETWORK FOR POWER QUALITY DISTURBANCES CLASSIFICATION

***Faqih Rofii*** ✉
*Departement of Physics*[1]
*Departement of Electrical Engineering*[2]
*faqihs3fisika@student.ub.ac.id*

***Agus Naba***
*Departement of Physics*[1]

***Hari Arief Dharmawan***
*Departement of Physics*[1]

***Fachrudin Hunaini***
*Departement of Electrical Engineering*[2]

[1]*Universitas Brawijaya Malang*
*Jl. Veteran, Malang, Jawa Timur, Indonesia, 65145*

[2]*Universitas Widyagama Malang*
*35 Jl. Borobudur Malang, Jawa Timur, Indonesia, 65142*

✉**Corresponding author**

**Abstract**

The complexity of the electric power network causes a lot of distortion, such as a decrease in power quality (PQ) in the form of voltage variations, harmonics, and frequency fluctuations. Monitoring the distortion source is important to ensure the availability of clean and quality electric power. Therefore, this study aims to classify power quality using a neural network with empirical mode decomposition-based feature extraction. The proposed method consists of 2 main steps, namely feature extraction, and classification. Empirical Mode Decomposition (EMD) was also applied to categorize the PQ disturbances into several intrinsic mode functions (IMF) components, which were extracted using statistical parameters and the Hilbert transformation. The statistical parameters consist of mean, root mean squared, range, standard deviation, kurtosis, crest factor, energy, and skewness, while the Hilbert transformation consists of instantaneous frequency and amplitude. The feature extraction results from both parameters were combined into a set of PQ disturbances and classified using Multi-Layer Feedforward Neural Networks (MLFNN). Training and testing were carried out on 3 feature datasets, namely statistical parameters, Hilbert transforms, and a combination of both as inputs from 3 different MLFNN architectures. The best results were obtained from the combined feature input on the network architecture with 2 layers of ten neurons, by 98.4 %, 97.75, and 97.4 % for precision, recall, and overall accuracy, respectively. The implemented method is used to classify PQ signals reliably for pure sinusoids, harmonics with sag and swell, as well as flicker with 100 % precision.

**Keywords:** Power Quality, EMD, Hilbert Transformation, statistical parameters, Neural Networks, Accuracy.

**DOI: 10.21303/2461-4262.2022.002046**

## 1. Introduction

The electric power system generates electrical energy which is delivered to customers at an accepTable voltage and current levels. However, as the number of devices connected to the system grows, such as electronics, non-linear loads, and inverters, this process is becoming more complex. Furthermore, the increasing and widespread use of nonlinear loads in industrial environments, such as electric motor speed regulation, power supplies, lighting, transformers, and converters, causes power quality (PQ) issues in the electricity network. PQ disturbances harm industrial operations, resulting in production losses, manufacturing disruptions, product damage, wasted energy, and reduced equipment life [1, 2]. Subsequently, the rise in the use of sensitive electronic components, such as computers, programmable logic controllers, protective equipment, and relays increases the

electrical power consumption with continuous supply and high power quality, thereby demanding that consumers provide uninterrupTable power supplies and stabilizers at high costs [3].

The provision of renewable energy sources based on biomass, wind, solar and tidal waves mostly requires inverters for the conversion of electricity quantities. There are several advantages associated with the inverter, however, its output voltage contains a large number of unwanted harmonics, which harms the mechanical and electrical components of the system [4], affect the quality of the electricity network output power, voltage fluctuations, and malfunctions in the devices connected to the network [5]. The integration of renewable energy into the existing power grid poses difficult technical challenges. An example is the PQ problem in the form of voltage and frequency fluctuations caused by its variability and harmonics generated by power electronic devices used in renewable energy generation, which is an important aspect in its integration [6]. The availability of these sources encourages integration and connection with the existing electricity distribution network, thereby creating a smart grid concept with PQ as an important aspect that cannot be ignored because it ensures the necessary compatibility between all the equipment connected to the network [7].

The smart grid network consists of two-way communication between customers and electricity providers, through power line communication. The frequency range used coincides with supraharmonic emissions sourced from power and energy-saving electronic equipment, thereby creating disturbances in the network with varying data transfer rates. Amaripadath carried out research for measuring and detecting supraharmonic emissions in smart grids [8]. This research also describes dynamic state analysis parameters for measurement and configuration. According to Amaripadath, the system experiences a basic shift in the main operation, such as a change from direct power flow in the form of alternating current (AC) to a direct current (DC) and AC with a wider frequency range. Therefore, PQ is an important parameter used to analyze the effects of power interactions and future changes on the network [9].

PQ monitoring [10] consists of 2 main subjects namely the development of a power quality index to measure the electrical supply and detection of disturbances to determine the electric system condition. The power quality index is the basis of the PQ standard used to describe the negative impact of electrical disturbances, in the form of frequency deviation, supply voltage variation, flicker, transient voltage, harmonics, etc. The second is the traditional index, namely the peak value, factor, total harmonic distortion, power factor, and the proposed new index, which consists of instantaneous distortion energy ratio, frequency, burst index, etc. PQ is a quality combination of current and voltage, which deals with their respective ideal deviations. Furthermore, it depends on the quality of supply, as a combination of voltage and non-technical aspects of the interaction between the power grid and the customer [11].

Classification of power quality disturbances is needed as a first step to identify and mitigate sources of distortion [12]. Therefore, it is necessary to monitor PQ disturbances to provide clean power as suggested by IEEE [13, 14]. Several studies on the detection and classification of PQ disturbances have been conducted, including the generation of a mathematical model using the discrete wavelet transform-fast Fourier approach [15], fuzzy-wavelets [16], support vector machine algorithms [17], analysis of the real signal database distorted by the disturbance of the measurement system results with the unsupervised classification approach [18] and an intelligent measurement [19]. EMD method and Hilbert transformation were developed for assessment [20]. Probabilistic neural network is used as a mapping function to identify different disturbance classes.

In [16] developed an intelligent system for the PQ disturbances diagnosis in a modular form. Extraction of the stress waveform characteristics was carried out through the combined use of discrete wavelet transform (DWT), multiresolution analysis (MRA), and entropy norm (EN). Meanwhile, the classification process was conducted using the fuzzy-ARTMAP neural network. In line with the development of data acquisition techniques and equipment, this system promotes ideas and efforts for the characterization and classification of PQ. According to [21], a combined knowledge of PQ problems, signal processing techniques, and artificial intelligence is needed to provide solutions [21]. The events are generally non-linear, non-stationary, and contain noise, with

several techniques developed for the analysis of non-stationary signals or data, with empirical mode decomposition as the most reliable [22]. EMD has been widely developed for the analysis of PQ events, such as harmonics, sag, swell, and flicker compared to other methods such as S-transformation [20].

Although preliminary studies [15, 17–19] have been able to classify PQ disturbances, the feature extraction method developed only uses statistical parameters and power distribution. Another shortcoming associated with these studies is the classification of the number of disturbances as few and not multi. This research is a continuation of the previous discussion on EMD-based PQ disturbances analysis and statistical parameters [23]. The proposed novelties are:

1. Development of feature extraction methods for various types of PQ disturbances signals using the EMD method, Hilbert transform and statistical parameters, such as mean, root mean squared, range, standard deviation, kurtosis, crest factor, energy, and skewness.

2. Development of Feedforward Neural Networks (FNN) for the classification of its signals.

## 2. Materials and methods

The term PQ is generally used to define the various electromagnetic phenomena that occur in power system networks. The ability of a power system to provide voltage, current, and frequency signals without distortion is referred to as power supply quality [24]. According to IEC 61000 Series, PQ is defined as systems, equipment, and devices capable of functioning in an electromagnetic environment without causing intolerable electromagnetic disturbances to all objects in their environment. Meanwhile, according to IEEE 1159:2009, IEEE 1100:2005, it is the concept of powering and grounding in the operation of electronic equipment compatible with supplies and other connected equipment.

The smooth operation of electrical equipment can be used to determine the extent to which a power supply is compatible and measure the smooth operation of its load. PQ disturbances, according to the IEEE 1159-1995 standard [25], include transients, interrupts, sag, and swells, frequency variations, undervoltages and overvoltages, and steady-state variations (harmonic, notch, and blinking). Meanwhile, the IEEE 1459-2010 standard specifies the amount of electric power in sinusoidal, non-sinusoidal, balanced, and unbalanced conditions [26].

The types of disturbances include voltage variations, harmonics, and frequency fluctuations. Voltage variation is defined as a deviation from the nominal voltage that lasts both short (milliseconds) and long (more than one minute). Dips/sags, spikes/surges, and swells are examples of short-duration voltage, whereas flicker (voltage fluctuation), undervoltage, overvoltage, and interruption are examples of long-duration voltage. Sag is a decrease in the value of the RMS voltage in the range of 10-90 % within a period of 0.5 cycles to less than one minute. A spike is a high instantaneous voltage that rapidly occurs within a short duration. Meanwhile, swell is an increase in the value of the RMS voltage in the range of 110–180 % within a period of 0.5 cycles to less than one minute. Harmonics are periodic sinusoidal distortions of supply voltage or load current and an integer multiple of the power supply's AC voltage and current. The deviation of the system's frequency from an accepTable standard nominal value (50 or 60 Hz) due to power dissimilarity in the load is referred to as frequency fluctuation. Fluctuations that exceed the tolerance value of 5 % are harmful to the power system and can lead to its collapse.

An integrated mathematical model consisting of sinusoidal signal distortion used to derive various PQ disturbance equations has been proposed by [27]. **Table 1** provides a mathematical model of the pure sinusoidal signal and PQ disturbance equation.

The detailed parameters of the PQ disturbances mathematical model in **Table 1** are shown in the reference research [27].

Since PQ disturbance waves are mostly non-stationary and noisy in nature, their identification and analysis require a robust and accurate method. The Fourier transform (FT) is the most commonly used algorithm for signal analysis. The Fourier spectral analysis has some significant limitations, including the requirement that the data be stationary with a linear system to obtain a correct spectrum. A Short-Time Fourier Transform (STFT) with a windowing technique was also developed to determine the FT on a smaller area of the entire signal [28].

**Table 1**
PQ disturbances mathematical model

| Class | PQ Disturbances | Equations |
|---|---|---|
| 1 | Pure Sinusoidal | $v(t)=A\sin(\varpi t+\varphi)$ |
| 2 | Sag | $v(t)=A\left(1-\alpha\left(u(t-t_1)-u(t-t_2)\right)\right)\sin(\varpi t+\varphi)$ |
| 3 | Swell | $v(t)=A\left(1-\beta\left(u(t-t_1)-u(t-t_2)\right)\right)\sin(\varpi t+\varphi)$ |
| 4 | Interruption | $v(t)=A\left(1-\rho\left(u(t-t_1)-u(t-t_2)\right)\right)\sin(\varpi t+\varphi)$ |
| 5 | Transient | $v(t)=A\left[\sin(\varpi t-\varphi)-\psi\left(e^{-750(t-t_a)}-e^{-334(t-t_a)}\right)\left(\left(u(t-t_a)-u(t-t_b)\right)\right)\right]$ |
| 6 | Oscillatory Transient | $v(t)=A\left[\sin(\varpi t-\varphi)+\beta e^{-(t-t_1)/\tau}\sin\left(w_n(t-t_I)-\vartheta\right)\left(\left(u(t-t_{II})-u(t-t_I)\right)\right)\right]$ |
| 7 | Harmonics | $v(t)=A\left[\sin(\varpi t+\varphi)+\sum_{n=3}^{7}\alpha_n\sin(n\varpi t-\vartheta_n)\right]$ |
| 8 | Harmonics With Sag | $v(t)=A\left(1-\alpha\left(u(t-t_1)-u(t-t_2)\right)\right)\sin(\varpi t+\varphi)\left[\sin(\varpi t+\varphi)+\sum_{n=3}^{7}\alpha_n\sin(n\varpi t-\vartheta_n)\right]$ |
| 9 | Harmonics With Swell | $v(t)=A\left(1-\beta\left(u(t-t_1)-u(t-t_2)\right)\right)\sin(\varpi t+\varphi)\left[\sin(\varpi t+\varphi)+\sum_{n=3}^{7}\alpha_n\sin(n\varpi t-\vartheta_n)\right]$ |
| 10 | Flicker | $v(t)=A\left[1+\lambda\sin(w_f t)\right]\sin(\varpi t-\vartheta)$ |

The Hilbert Huang Transform (HHT), which consists of two processes, is one of the tools for analyzing non-stationary complex waveforms with excellent time resolution [23]. First, the signal is decomposed into IMFs using EMD process, which has a significant effect on the instantaneous amplitude, frequency, and phase of the analyzed signal components. Second, the Hilbert Transform is applied to each of the IMFs that are granting loans. Based on scale separation, EMD decomposes a time series into several IMFs. Scale separation is defined as the minimum or maximum distance between two successive local extremes. The EMD algorithm is shown below [23]:

1. Identify all local maximum and minimum values of data ($X(t)$).
2. Determine the top ($X_{up}(t)$) and bottom covers ($X_{low}(t)$) using cubic spline interpolation.
3. Calculate the mean ($m(t)$) for the top and bottom covers with (1):

$$m(t)=\left(X_{up}(t)+X_{low}(t)\right)/2. \quad (1)$$

4. Find the difference $C(t)$ between the data signal and the mean with (2):

$$C(t)=X(t)-m(t). \quad (2)$$

5. Check the value of $C(t)$ using the following conditions.

If $C(t)$ satisfies two IMF criteria, then $h(t)=c(t)$ is the IMF component of the signal. Otherwise, substitute $X(t)$ with the residue resulting from Equation (3):

$$r(t)=X(t)-C(t). \quad (3)$$

There are two criteria for producing an IMF, namely:

– in all data series, the number of extrema (maximum and minimum sum) and the data series that equals zero need to be similar or differ by at most 1;

– at each point, the mean of the local maximum and minimum value covers should equal zero.

If $C(t)$ is not a IMF, replace $X(t)$ with $C(t)$.

Repeat steps 1–5 until a residue that meets the iteration termination criteria is obtained.

The Hilbert transform of a real-valued $x(t)$ time-domain signal is another real-valued $\hat{x}(t)$ time-domain signal, denoted by an analysis signal $z(t) = x(t) + \hat{x}(t)$, where:

$$\hat{x}(t) = H\left[x(t)\right] = \int_{-\infty}^{\infty} \frac{x(\tau)}{\pi(t-\tau)}. \tag{4}$$

The dominant function of time $t$ is in the range of $-\infty < t < \infty$. The Hilbert transform of a signal produces an orthogonal signal that is 90 degrees off by the original.

The instantaneous amplitude of the $x(t)$ signal is defined as follows:

$$A(t) = \left[x^2(t) + j\hat{x}(t)\right]^{1/2}. \tag{5}$$

The $x(t)$ signal's instantaneous frequency is defined as follows:

$$f_0 = \frac{1}{2\pi t}\tan^{-1}\left[\frac{\hat{x}(t)}{x(t)}\right]. \tag{6}$$

In general, the proposed PQ disturbance classification method consists of two main steps, the first is preprocessing in the form of feature extraction, while the second is classification. Furthermore, the first step uses the EMD method to decompose its data into several intrinsic mode functions (IMF) components. The feature extraction on IMF is done by using statistical parameters and Hilbert transformation. Feature extraction using statistical parameters produces values in the form of mean, root mean squared, range, standard deviation, kurtosis, crest factor, energy, and skewness, while the Hilbert transformation produces the instantaneous frequency and amplitude of each IMF. The feature extraction result from the two is then combined into a set of PQ disturbances. The second step is to develop an artificial neural network (ANN) structure to classify the type where the input is a feature that has been obtained. The sequence of feature extraction steps is shown in **Fig. 1**.

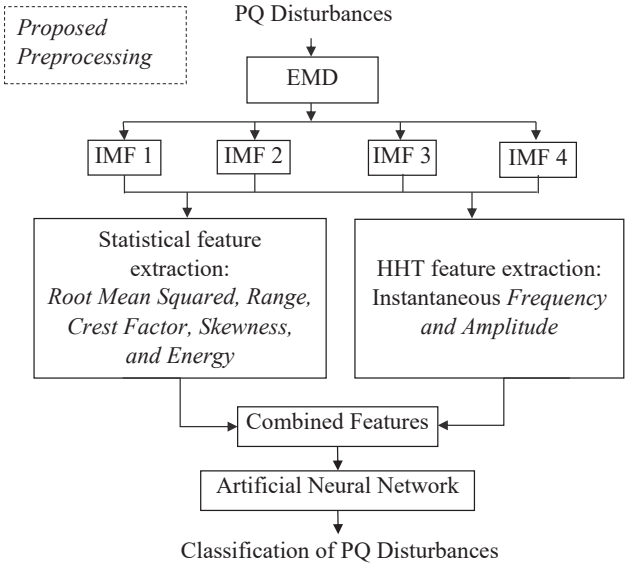


**Fig. 1.** Classification of PQ Disturbances using Neural Network

PQ disturbances are data from pure sinusoidal, sag, swell, interruption, transient, oscillatory transient, harmonics, harmonics with sag, and flicker signals, which are decomposed using EMD to obtain the IMF composition. This research considers the first 4 IMFs for feature extraction and calculates their statistical values. Furthermore, the Hilbert transform technique was used to obtain features of the PQ disturbances signal in the form of instantaneous amplitude and frequency.

The following are the steps for extracting the features of PQ disturbances using statistical parameters and the Hilbert transformation:

1) Using the *N*-dataset, generate pure *X* sinusoidal signals and PQ disturbances:

$$X = \left[ x_{1,1}(t) x_{1,2}(t) x_{1,3}(t) \ldots x_{1,N}(t) \quad x_{2,1}(t) x_{2,2}(t)\ x_{2,3}(t) \ldots x_{M,N}(t) \right]. \tag{7}$$

2) Decompose *X* data using EMD to generate IMF set:

$$IMF_X = emd(X). \tag{8}$$

3) For each IMF, use statistical parameters such as mean, root mean squared, range, standard deviation, kurtosis, crest factor, energy, and skewness:

$$\text{Mean} \rightarrow M = \bar{x} = \frac{1}{N} \sum_{n=1}^{N} IMF_X, \tag{9}$$

$$\text{Standard deviation} \rightarrow S = \left[ \frac{1}{N-1} \sum_{n=1}^{N} \left( IMF_X - \bar{x} \right)^2 \right]^{\frac{1}{2}}, \tag{10}$$

$$\text{Root means square} \rightarrow RMS = \left[ \frac{1}{N} \sum_{n=1}^{N} IMF_X^2 \right], \tag{11}$$

$$\text{Range} \rightarrow R = \max\left( IMF_X \right) - \min\left( IMF_X \right), \tag{12}$$

$$\text{Crest Factor} \rightarrow CF = \frac{IMF_X \ \max}{RMS}, \tag{13}$$

$$\text{Kurtosis} \rightarrow \quad K = \frac{1}{S^4 N} \sum_{n=0}^{N-1} \left( IMF_X - \bar{x} \right)^4, \tag{14}$$

$$\text{Skewness} \rightarrow \quad SK = \frac{1}{S^3 N} \sum_{n=0}^{N-1} \left( IMF_X - M \right)^3, \tag{15}$$

$$\text{Energy} \rightarrow \quad E = \sum_{n=1}^{N} \left( \left| IMF_X \right|^2 \right). \tag{16}$$

4) To obtain the instantaneous frequency and amplitude, apply the Hilbert transform to each IMF:

$$\widehat{IMF}(t) = H\left[ IMF(t) \right] = \int_{-\infty}^{\infty} \frac{IMF(\tau)}{\pi(t-\tau)}. \tag{17}$$

The instantaneous amplitude of the *IMF*(*t*) signal is defined as follows:

$$A_{IMF}(t) = \left[ IMF^2(t) + j\widehat{IMF}(t) \right]^{1/2}. \tag{18}$$

The instantaneous frequency of the x(t) signal is expressed as follows:

$$f_0 = \frac{1}{2\pi t} \tan^{-1} \left[ \frac{\widehat{IMF}(t)}{IMF(t)} \right]. \tag{19}$$

After feature extraction, 32 statistical features were derived from the first 8 multiplied by 4 IMFs. Furthermore, 8 features of the Hilbert transformation derived from the first

2 features were multiplied by 4 IMFs. In the end, a total of 40 combined statistical features and Hilbert transformations were obtained which are expressed as $Ft1_1$, $Ft1_2$, $Ft1_3$,… $Ft4_{10}$ as summarized in **Table 2**.

**Table 2**
Features obtained by statistical parameters and Hilbert Transformation

| Features | *IMF*-1 | *IMF*-2 | *IMF*-3 | *IMF*-4 |
|---|---|---|---|---|
| Mean | $Ft1_1$ | $Ft2_1$ | $Ft3_1$ | $Ft4_1$ |
| Standard deviation | $Ft1_2$ | $Ft2_2$ | $Ft3_2$ | $Ft4_2$ |
| Root Mean Squared | $Ft1_3$ | $Ft2_3$ | $Ft3_3$ | $Ft4_3$ |
| Range | $Ft1_4$ | $Ft2_4$ | $Ft3_4$ | $Ft4_4$ |
| Crest Factor | $Ft1_5$ | $Ft2_5$ | $Ft3_5$ | $Ft4_5$ |
| Kurtosis | $Ft1_6$ | $Ft2_6$ | $Ft3_6$ | $Ft4_6$ |
| Skewness | $Ft1_7$ | $Ft2_7$ | $Ft3_7$ | $Ft4_7$ |
| Energy | $Ft1_8$ | $Ft2_8$ | $Ft3_8$ | $Ft4_8$ |
| Inst. Frequency | $Ft1_9$ | $Ft2_9$ | $Ft3_9$ | $Ft4_9$ |
| Inst. Amplitude | $Ft1_{10}$ | $Ft2_{10}$ | $Ft3_{10}$ | $Ft4_{10}$ |

The second step is to classify the type of PQ disturbances by developing Multi-Layer Feed-forward MLF Neural Networks (MLFNN), which is an artificial neural network consisting of neurons arranged into many layers. The first layer is called the input, and the last is the output, and between both is the hidden layer with its number dependent on the problem to be solved. The input layer is connected to the hidden by the set of weights, while the hidden layer is connected to the output by weights to the feed-forward system [29]. MLF neural network is widely used for accurate diagnosis [30], estimation [31], forecasting [32] and classification [33].

Based on experiments using Matlab 2019b, MLFNN was used with the architecture as shown in **Fig. 2**. It consists of 1 input, 2 hidden, and 1 output layer. The input has *N* feature columns, each hidden and output layer contains 10 neurons, and the final section has 10 outputs. The transfer function in hidden layers 1 and 2 is 'tansig' while the output is 'softmax'. Tansig also known as hyperbolic tangent sigmoid is a function to calculate the output of input in the range –1 to +1. This function is a better tradeoff than the tanh function in Matlab-implemented neural networks, so it is commonly used as a transfer function in a network's hidden layer [34]. Softmax is a mapping function from input real numbers, that normalizes and makes the probability distribution in the range (0, 1). A larger input component corresponds to a greater probability. It is also often used in neural networks at the output layer to represent categorical distributions, such as object classification [35].

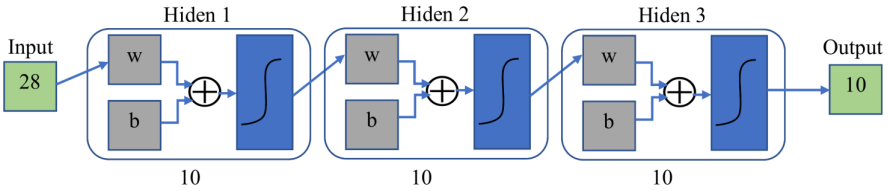


**Fig. 2.** MLF Neural Network Architecture

The network consists of many layers where each has a weight matrix *W*, bias vector *b*, output vector a, and activation function f. **Fig. 5** shows how the MLF neural network architecture is used to identify and classify ten different types of PQ signals. PQ data generated as many as 1,500 different variations for each type of PQ, which means that there are 10×1,500 data. By applying the data preprocessing according to the steps in **Fig. 1**, 40 features×1,500 data columns

were obtained. The ratio of the dataset distribution used as training, validation, and testing data is 0.75, 0.15, and 0.15, respectively. To train the network, the Trainlm backpropagation algorithm was used, which was chosen due to its supervised and optimized standard in achieving the desired target. It also used the Hessian matrix approach to update the weight [35]. This optimization algorithm is better than the Gauss-Newton algorithm (GNA) and the gradient descent (GD), although it requires more memory. The performance of trainlm is expressed in terms of mean or sum of squared error (MSE) using Jacobian for error calculation. MSE is calculated as shown in equation (17).

$$MSE = \frac{1}{N}\sum_{i=1}^{N}(e_i)^2 = \frac{1}{N}\sum_{i=1}^{N}(t_i - a_i)^2, \tag{17}$$

where $N$ is the number of data, $e_i$ is the $i$-th error as a result of the $t_i$ target value minus the $a_i$ output value.

## 3. Results and discussion

The dataset consists of a pure sinusoidal signal and a PQ disturbances as shown in **Fig. 3**. It is generated randomly with a uniform distribution through computer simulation using Matlab 2019a. Based on the signal mathematical model [27], ten classes of PQ signals are generated, each with 1,500 data samples, for a total of 15,00. The sampling frequency of 16 kS/sec, the number of 100 samples per class, the amplitude of 1 p. u., and the fundamental frequency of 50 Hz with 10 cycles are the main parameters of the generated dataset. The data samples are arranged by class, as shown in **Table 1**.

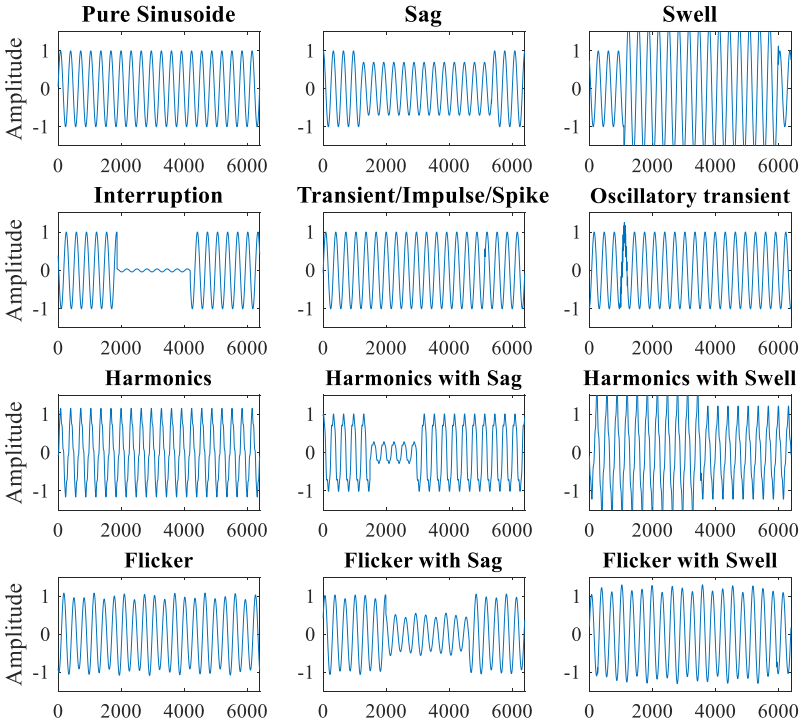


**Fig. 3.** Signals of pure sinusoidal and power quality disturbances

Furthermore, feature extraction is applied to the dataset to obtain the first 4 IMFs by using EMD as shown in **Fig. 4**. This is because most of the frequency content of the PQ disturbances signal lies in the first 4 oscillation modes. By calculating the statistical parameters and applying the Hilbert transform to each IMF, 40 features×10 classes×1,500 data columns were obtained. The obtained feature dataset is divided into sub-datasets for training, validation, and testing.

The target output is formed by creating a matrix with the size of 10 classes×1,500 feature data, where each class output is expressed in one hot encoding.

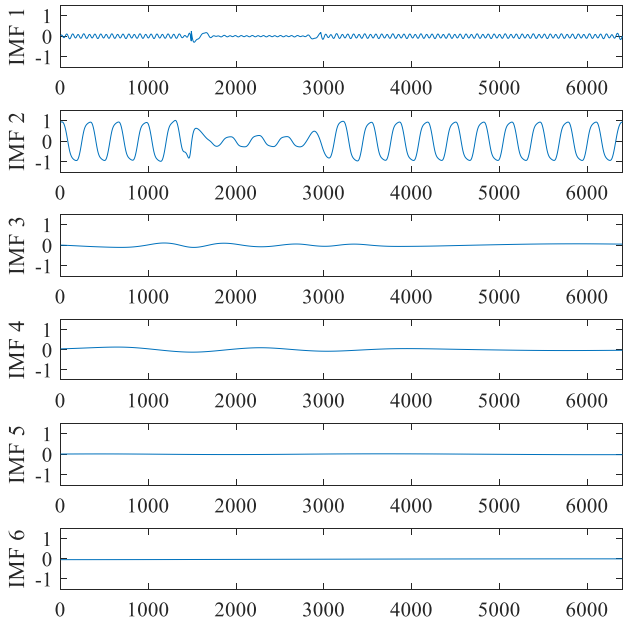


**Fig. 4.** IMF of harmonics with sag signal

Before training the network, the weights and biases were assigned a random initial value. Training stops when a maximum number of epochs (repetitions) is reached, performance is minimized to the goal, the gradient of performance falls below min grad, and validation performance increases more than max fail times. The training process uses a computer with a Core i5-6200U processor specification, 16 GB RAM, and Matlab 2019b. This research determined the classification accuracy of network outputs as a result of processing inputs with different network architectures. The network input consists of 3 types of features, namely statistics, Hilbert transformation, and a combination of both. Meanwhile, the network architecture consists of several hidden layers and different neurons Furthermore, there is no precise formula for calculating the number of neurons in a hidden layer. The network architecture is formed by input layer, hidden layer 1, hidden layer 2, and an output layer with the structure *N*-input – 10–10–10-output, *N*-input – 15–15–10-output, *N*-input – 20–20–10-output, and *N*-input – 25–25–10-output. In this case, the order of structure from the architecture is expressed as 1, 2, and 3.

This research conducts 3 types of training and testing based on the type of input and network architecture, as follows:

1. First, training and testing are carried out by providing input statistical features on networks with architectures 1, 2, and 3.

2. Second, the training and testing are carried out by providing input features of the Hilbert transformation on the network with architectures 1, 2, and 3.

3. Third, training and testing are carried out by providing input statistical features-Hilbert transformation on networks with architectures 1, 2 and 3.

**Tables 3**–**5** show the training and testing of the 3 types of training, which tend to produce network weights after reaching several epochs. The weights and network architecture obtained from the training process are then used to determine the testing data to accurately classify the PQ. The classification accuracy of each class and the whole is obtained from the confusion matrix after testing all the data. There are 10 and 9 classes of PQ signals and disturbances, respectively as shown in **Table 1**. To avoid underfitting, the number of datasets is enlarged to 1,500 per case. Meanwhile, to avoid overfitting, it is divided into training, validation, and testing. Furthermore, after each training, the validation process is carried out to validate the model and prevent overfitting.

**Table 3**

Precision, recall, and accuracy of network classification with statistical feature input

| Number of Features | Network Architecture (neurons) | Performance parameters | Class of PQ | | | | | | | | | |
|---|---|---|---|---|---|---|---|---|---|---|---|---|
| | | | 1 | 2 | 3 | 4 | 5 | 6 | 7 | 8 | 9 | 10 |
| | | Precision (%) | 86.8 | 90.3 | 98.4 | 84.7 | 93.6 | 97.0 | 98.7 | 98.2 | 99.5 | 99.5 |
| 32 | 10–10–10 | Recall (%) | 100 | 85.4 | 96.4 | 89.6 | 82.2 | 96.6 | 99.6 | 99.1 | 97.0 | 100 |
| | | Overall Accuracy (%) | | | | | | | | | | 94.6 |
| | | Precision (%) | 85.8 | 79.6 | 95.0 | 75.1 | 93.7 | 88.9 | 100 | 90.7 | 95.7 | 97.5 |
| 32 | 15–15–10 | Recall (%) | 100 | 73.2 | 96.9 | 85.6 | 81.3 | 92.7 | 75.8 | 96.4 | 97.5 | 100 |
| | | Overall Accuracy (%) | | | | | | | | | | 89.7 |
| | | Precision (%) | 85.5 | 75.4 | 96.9 | 79.0 | 96.3 | 94.4 | 100 | 92.4 | 97.4 | 98.0 |
| 32 | 20–20–10 | Recall (%) | 100 | 79.6 | 95.5 | 84.4 | 82.2 | 94.4 | 84.1 | 96.9 | 94.9 | 100 |
| | | Overall Accuracy (%) | | | | | | | | | | 91.1 |

**Table 4**

Precision, recall, and accuracy of network classification with Hilbert transform input

| Number of Features | Network Architecture (neurons) | Performance parameters | Class of PQ | | | | | | | | | |
|---|---|---|---|---|---|---|---|---|---|---|---|---|
| | | | 1 | 2 | 3 | 4 | 5 | 6 | 7 | 8 | 9 | 10 |
| | | Precision (%) | 71.0 | 88.2 | 97.4 | 87.6 | 95.5 | 99.6 | 100 | 100 | 99.5 | 91.0 |
| 12 | 10–10–10 | Recall (%) | 100 | 86.6 | 99.0 | 85.3 | 78.5 | 99.6 | 93.4 | 99.1 | 100 | 78.2 |
| | | Overall Accuracy (%) | | | | | | | | | | 92.1 |
| | | Precision (%) | 66.8 | 91.8 | 96.5 | 89.3 | 95.1 | 99.6 | 99.5 | 97.7 | 98.0 | 91.0 |
| 12 | 15–15–10 | Recall (%) | 100 | 88.0 | 97.4 | 91.2 | 82.2 | 98.7 | 95.2 | 97.3 | 97.5 | 63.4 |
| | | Overall Accuracy (%) | | | | | | | | | | 91.4 |
| | | Precision (%) | 58.6 | 88.5 | 95.7 | 92.1 | 85.2 | 100 | 100 | 98.7 | 99.5 | 48.4 |
| 12 | 20–20–10 | Recall (%) | 44.7 | 86.0 | 90.8 | 84.0 | 77.0 | 99.6 | 95.5 | 99.6 | 98.5 | 77.1 |
| | | Overall Accuracy (%) | | | | | | | | | | 85.6 |

**Table 5**

Precision, recall, and accuracy of network classification with Statistics – Hilbert transformation input

| Number of Features | Network Architecture (neurons) | Performance parameters | Class of PQ | | | | | | | | | |
|---|---|---|---|---|---|---|---|---|---|---|---|---|
| | | | 1 | 2 | 3 | 4 | 5 | 6 | 7 | 8 | 9 | 10 |
| | | Precision (%) | 97.4 | 94.3 | 96.5 | 94.2 | 94.3 | 99.4 | 100 | 98.8 | 100 | 99.3 |
| 28 | 10–10–10 | Recall (%) | 100 | 95.5 | 99.3 | 95.6 | 96.8 | 96.3 | 92.8 | 100 | 98.5 | 100 |
| | | Overall Accuracy (%) | | | | | – | | | | | 97.4 |
| | | Precision (%) | 97.5 | 95.9 | 95.7 | 88.4 | 98.0 | 98.7 | 99.4 | 98.8 | 100 | 97.9 |
| 28 | 15–15–10 | Recall (%) | 100 | 89.7 | 96.4 | 96.3 | 97.4 | 98.1 | 94.5 | 99.4 | 99.3 | 100 |
| | | Overall Accuracy (%) | | | | | | | | | | 97.1 |
| | | Precision (%) | 98.1 | 93.6 | 94.1 | 90.2 | 97.3 | 99.4 | 97.6 | 98.8 | 98.5 | 98.5 |
| 28 | 20–20–10 | Recall (%) | 100 | 94.2 | 90.7 | 94.9 | 92.9 | 98.8 | 97.6 | 98.8 | 98.5 | 100 |
| | | Overall Accuracy (%) | | | | | | | | | | 96.7 |

The confusion matrix is used as a basis for measuring the performance of model testing towards the dataset. It also provides information on the comparison of the classification results performed by the model in terms of accuracy, precision, and recall. To obtain these parameters, it is necessary to determine the predicted and actual values. The True Positive (TP), True Negative (TN), False Positive (FP), and False Negative (FN) are positive, negative, negative, and positive data predicted to be correct, true, positive, and negative, respectively.

$$\text{Total accuracy} = \frac{TP}{\text{Total dataset}}, \tag{20}$$

$$\text{Precision} = \frac{TP}{TP + FP}, \tag{21}$$

$$\text{Total Precision} = \frac{\sum_{i=1}^{N} \text{Precision}(i)}{\sum \text{class}}, \tag{22}$$

$$\text{Recall} = \frac{TP}{TP + FN}, \tag{23}$$

$$\text{Total Recall} = \frac{\sum_{i=1}^{N} \text{Recall}(i)}{\sum \text{class}}. \tag{24}$$

**Fig. 5** shows the confusion matrix of the output and target class of the testing data. There are 1,500 test data from 10 *PQ* signals with the row denoting the output or predicted class, while the column is the target or actual class. Diagonal cells are correctly classified observations. The rightmost column is precision (positive predictive value), the bottom row is recall (true positive) and the bottom-right cell is overall accuracy.

**Confusion Matrix**

| Output Class \ Target Class | 1 | 2 | 3 | 4 | 5 | 6 | 7 | 8 | 9 | 10 | |
|---|---|---|---|---|---|---|---|---|---|---|---|
| 1 | **156** 10.4% | **0** 0.0% | **0** 0.0% | **0** 0.0% | **3** 0.2% | **0** 0.0% | **0** 0.0% | **0** 0.0% | **1** 0.0% | **0** 0.0% | 97.5% 2.5% |
| 2 | **0** 0.0% | **139** 9.3% | **1** 0.1% | **3** 0.2% | **0** 0.0% | **1** 0.1% | **1** 0.1% | **0** 0.0% | **0** 0.0% | **0** 0.0% | 95.9% 4.1% |
| 3 | **0** 0.0% | **1** 0.1% | **133** 8.9% | **2** 0.1% | **0** 0.0% | **2** 0.1% | **1** 0.1% | **0** 0.0% | **0** 0.0% | **0** 0.0% | 95.7% 4.3% |
| 4 | **0** 0.0% | **0** 0.0% | **1** 0.1% | **129** 8.6% | **0** 0.0% | **0** 0.0% | **1** 0.1% | **0** 0.0% | **0** 0.0% | **0** 0.0% | 88.4% 11.6% |
| 5 | **0** 0.0% | **15** 1.0% | **2** 0.1% | **0** 0.0% | **147** 9.8% | **0** 0.0% | **1** 0.1% | **0** 0.0% | **0** 0.0% | **0** 0.0% | 98.0% 2.0% |
| 6 | **0** 0.0% | **0** 0.0% | **1** 0.1% | **0** 0.0% | **0** 0.0% | **153** 10.2% | **1** 0.1% | **0** 0.0% | **0** 0.0% | **0** 0.0% | 98.7% 1.3% |
| 7 | **0** 0.0% | **0** 0.0% | **0** 0.0% | **0** 0.0% | **0** 0.0% | **0** 0.0% | **156** 10.4% | **0** 0.0% | **0** 0.0% | **0** 0.0% | 99.4% 0.6% |
| 8 | **0** 0.0% | **0** 0.0% | **0** 0.0% | **0** 0.0% | **0** 0.0% | **0** 0.0% | **2** 0.1% | **165** 11.0% | **0** 0.0% | **0** 0.0% | 98.8% 1.2% |
| 9 | **0** 0.0% | **0** 0.0% | **0** 0.0% | **0** 0.0% | **0** 0.0% | **0** 0.0% | **0** 0.0% | **0** 0.0% | **135** 9.0% | **0** 0.0% | 100% 0.0% |
| 10 | **0** 0.0% | **0** 0.0% | **0** 0.0% | **0** 0.0% | **0** 0.0% | **0** 0.0% | **0** 0.0% | **0** 0.0% | **0** 0.0% | **143** 9.5% | 97.9% 2.1% |
| | 100% 0.0% | 89.7% 10.3% | 96.4% 3.6% | 96.3% 3.7% | 97.4% 2.6% | 98.1% 1.9% | 94.5% 5.5% | 99.4% 0.6% | 99.3% 0.7% | 100% 0.0% | 97.1% 2.9% |

**Fig. 5.** Confusion matrix for the testing dataset

Based on the confusion matrix in **Fig. 5**, the values for accuracy, precision, and recall are as follows:

$$\text{Acuracy} = \frac{148+148+133+136+146+168+156+171+136+124}{1500} = 0.977 = 97.7\ \%.$$

(21) is used to determine the precision value as follows:

$$\text{Precision}(PQ_1) = \frac{148}{148+3} = 0.977 = 98\ \%,$$

in the same way, will get the precision for $PQ_2$ until $PQ_{10}$, therefore the total precision obtained according to (22) is as follows:

$$\text{Total Precision} = \frac{86.8 + 90.3 + 98.4 + 84.7 + 93.6 + 97 + 98.7 + 98.2 + 99.5}{10} = 98.4\ \%.$$

Furthermore, the recall value is obtained through equation 23, as follows:

$$\text{Recall}\left(PQ_1\right) = \frac{148}{148} = 1 = 100\ \%$$

with a recall for $PQ_2$ until $PQ_{10}$, therefore the total recall obtained according to (24) is as follows:

$$\text{Recall total} = \frac{100 + 93.1 + 94.3 + 95.1 + 97.3 + 98.8 + 98.7 + 100 + 100 + 100}{10} = 97.7\ \%.$$

**Table 3** shows the precision, recall, and accuracy of network classification with a total of 32 input statistical features. The total accuracy performance on network architectures 1, 2, and 3 are 94.6 %, 89.7 %, and 91.1 %, respectively. **Table 4** shows the precision, recall, and accuracy of network classification with a total of 12 input features of the Filbert transformation. The total accuracy performance on network architecture 1, 2, and 3 are 92.1 %, 91.4 %, and 85.6 %, respectively. Meanwhile, **Table 5** shows the precision, recall, and accuracy of network classification with statistical feature input and Hilbert transform, with a total input of 28 features. The total accuracy performance on network architectures 1, 2, and 3 are 97.4 %, 97.1 %, and 96.7 %, respectively.

Network performance is measured by overall accuracy, the number of iterations (epochs), MSE, and the length of training time as shown in **Table 6**. The least epochs are obtained in the first network architecture with a combination of input and features. Meanwhile, the most number of epochs from the Hilbert transformation feature is 1,000. The lowest and highest MSE obtained from the combined features and Hilbert transformations are 0.00178 and 0.0159. Furthermore, the fastest training time was obtained from the combined features of 4 minutes 11 seconds and the longest from the Hilbert transformation feature of 14 minutes 17 seconds.

**Table 6**

Comparison of epochs, MSE, and time

| Input Features | Network Architecture (neurons) | epoch | MSE | Time |
|---|---|---|---|---|
| Statistics Parameters (SP) | 10–10–10 | 204 | 0.00745 | 6 M; 30 S |
| Hilbert Transforms (HT) | 10–10–10 | 1000 | 0.0159 | 14 M; 7 S |
| SP+HT | 10–10–10 | 200 | 0.00178 | 4 M; 9 S |

This research focuses on obtaining PQ signal feature extraction using the EMD method for PQ signal decomposition. Furthermore, it applied statistical parameters and Hilbert transformation to the first 4 IMFs to produce 28 selected features. MLFNN was used to classify 10 classes of PQ disturbances which were evaluated based on precision, recall, accuracy, number of epochs, MSE, and learning process time. The results of the evaluation obtained knowledge as follows:

1. A total of 10 PQ classes were detected and classified, namely pure sinusoidal, sag, swell, interruption, transient, oscillatory transient, harmonics, harmonics with sag, harmonics with the swell, and flicker.

2. Based on **Tables 3–5** and **Fig. 6**, the best overall accuracy is obtained from network architecture 1, at 94.6 %, 92.1 %, and 97.4 %, respectively as shown in **Fig. 6**. Furthermore, when compared to the overall accuracy of the 3 input features, the combined statistical parameter and Hilbert transformation feature had the highest overall accuracy of 97.4 %.

3. The highest precision and total recall were obtained from the combined features of statistical parameters and the Hilbert transform, by 98.4 % and 97.7 %, respectively.

4. **Table 6**, showed that the lowest epoch, MSE, and training time were obtained from the combined features of statistical parameters and the Hilbert transformation.

5. The implemented method can be used to detect and classify PQ signals reliably for pure sinusoids, harmonics with sag and swell, and flicker with a precision of 100 %.

The benchmarked approach using a real-life dataset published in the IEE-data port was used to carry out this research [36]. The dataset was generated from experimental measurements on a power grid with a frequency of 50 Hz at the University of Cadiz in 2011. It provided a set of the most common PQ disturbances in the form of real-life sag events with a sampling frequency of 20 kHz for testing experimentation and measurement instrumentation according to UNE-IEC as shown in **Fig. 7**, 61000-4-11:2005 and UNE-EN-50160:2011.

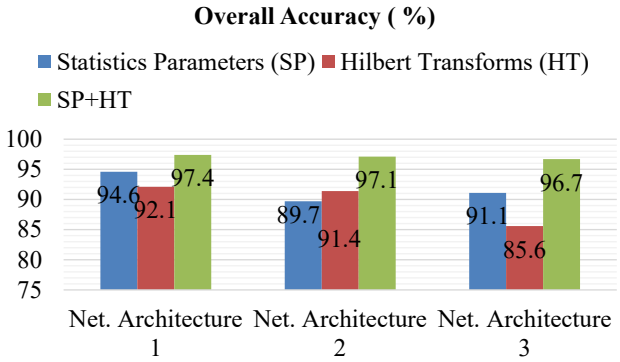


**Fig. 6.** The overall accuracy of all features input

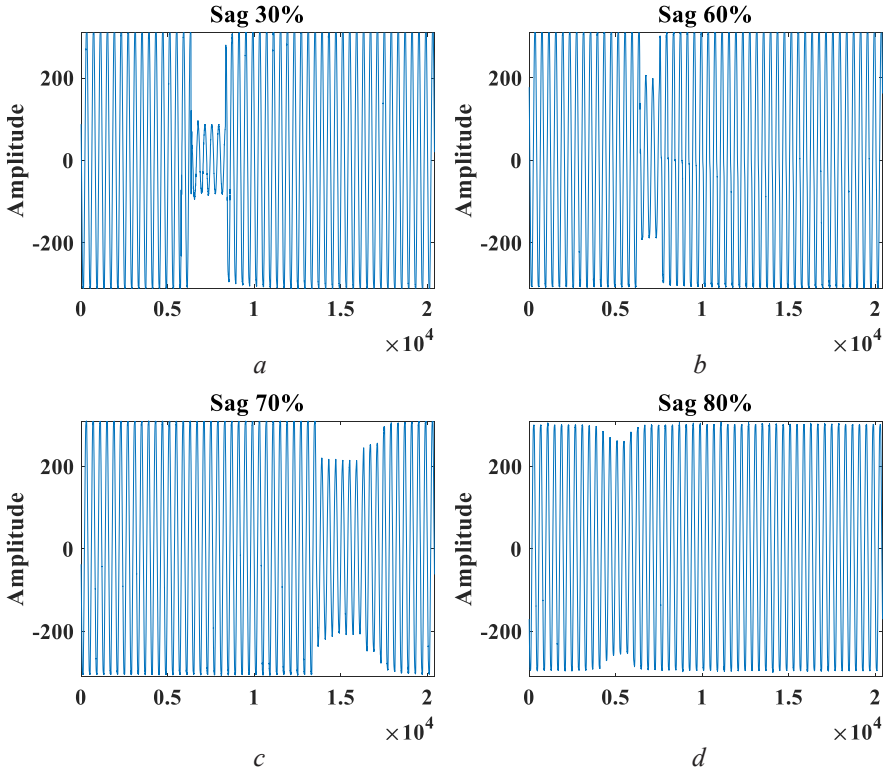


**Fig. 7.** Real-life power quality sag: *a* – 30 %; *b* – 60 %; *c* – 70 %; *d* – 80 %

The trained network is then applied to test the input data containing 30 %, 60 %, 70 %, and 80 % real-life sag as shown in **Fig. 7**. Each input data after being preprocessed is analyzed

by the network to obtain the PQ class type classification output. At 30 % real-life sag dataset produces 14 IMF components with frequencies in the range of 1 to 3.7 kHz. However, it only produces 6 IMF components when compared to the pure sag dataset with frequencies in the range of 1 to 50 Hz. **Fig. 8** shows the preprocessing results for the 30 % real-life sag dataset compared to the pure sag. The analysis result related to the network on the real-life sag signal preprocessed to produce a classification output is 'Harmonics with Sag.' This is understandable because the network is trained using a pure sag dataset where it only has a frequency component of 50 Hz as shown in **Fig. 7**. Meanwhile, the real-life sag dataset has several frequencies which are multiples of 50 Hz, therefore the network produces a classification output in the form of 'Harmonics with Sag.'

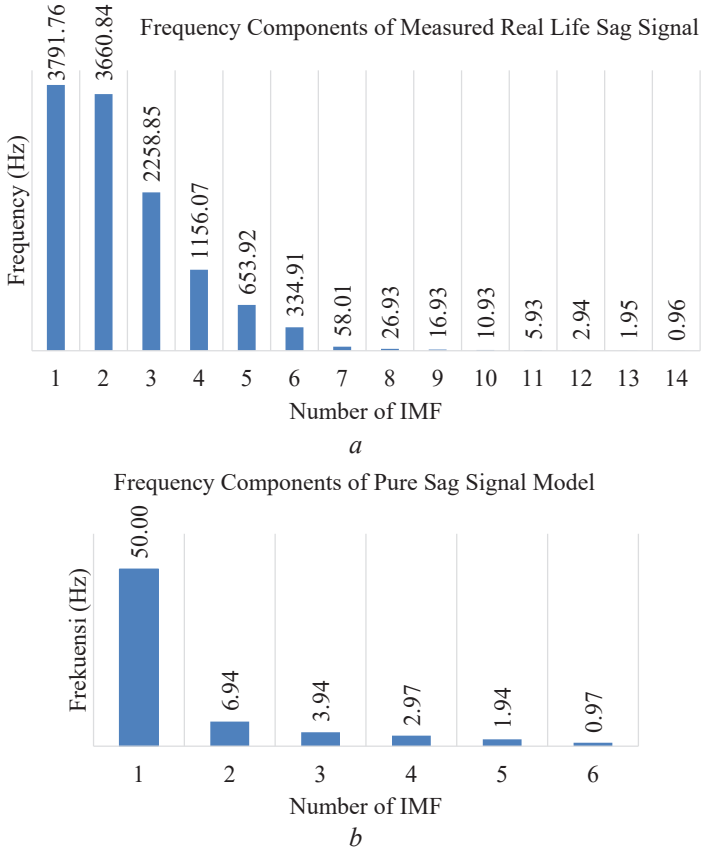


**Fig. 8.** Frequency component of: *a* – real-life signal; *b* – pure sag signal

**Fig. 8** shows the frequency component and IMF amount of the 30 % real-life sag signal. The figure shows that the frequency component of 50 Hz is found in the 7$^{th}$ IMF, while the 1st to 6th IMF contains its multiples. For further signal analysis, IMFs 1 to 6 are discarded and replaced with 7 to 14 as network input. The results of the network output on the filtered real-life sag signal produce a classification output in the form of 'Sag' as shown in **Fig. 8, *b***.

After filtering the 30 % real-life sag signal, it is then inputted into the neural network and the result is 'sag'. Another real-life sag dataset test that produces the correct classification output, without filters is 'sag'. The results of this test indicate that the trained network can detect and classify the types of PQ disturbances in the real data input of the measurement results. The detailed test results of each network architecture are summarized in **Table 7**.

The test results of trained networks on real-life datasets are evidence of the initial hypothesis that the EMD method and the developed statistical parameters and Hilbert Transforms can produce feature extraction as MLFNN input for PQ type classification. The features obtained significantly affect the accuracy of the model. The effect is shown by the values of R training, validation, test, and R-overall at 0.9917, 0.9918, 0.9771, and 0.9879, respectively. The output of the trained

network can detect and classify non-linear as well as non-stationary PQ signals with high accuracy. However, the trained network test on real-time measurement data is still limited to sag signals, due to the difficulty of obtaining data from other valid power quality signals.

**Table 7**
Classification accuracy results for a real signal

| PQ Disturbance | Accuracy | | |
|---|---|---|---|
| | Network Architecture 1 | Network Architecture 2 | Network Architecture 3 |
| Sag | 97.2 % | 94.6 % | 91.3 % |

This paper presents the advantages of feature extraction by developing the use of EMD, statistical parameters, and the Hilbert transformation. We have evaluated the performance of the developed method and obtained evidence that the approach is capable of detecting and classifying PQ disturbances with high accuracy. However, there are some shortcomings, such as the training data is synthetic, not real-life data, testing on real-life data is still only one class, and testing has not been carried out in real-time.

In future work, let's train neural networks with real-life data input measured from power loads containing various PQ disturbances. It is necessary a power electronics circuit that will generate many types of PQ disturbances and then capture the data with a data acquisition tool. Then, let's implement the trained network on a computer interface based on graphical user interface (GUI) software that is connected to a data acquisition tool to detect and classify various PQ disturbances in real-time.

## 4. Conclusions

In conclusion, this research described a novel approach of feature extraction and neural networks for the detection and classification of power quality signals by developing EMD methods, statistical parameters and Hilbert transforms. The main results were 28 selected features obtained from the decomposition of the power quality signal into the first 4 IMF and extracted into RMS values, range, crest factor, energy, instantaneous frequency, and amplitude. Furthermore, a network architecture in the form of MLFF was developed which consists of 10 to 15 neurons in the hidden layer for the classification of 10 PQ disturbance classes. The presented methodology showed satisfactory results for the classification process, which is expressed in terms of high precision, recall, and accuracy. Simple network architecture and training process without a long time is another reliability of this method. The trained network is proven to be able to predict input real-life datasets with high accuracy, although it is still limited to one case of power quality signal class, namely 'sag', due to the inadequate availability of real-life datasets.

**References**

[1] Muhamad, M. I., Mariun, N., Radzi, M. A. M. (2007). The Effects of Power Quality to the Industries. 2007 5th Student Conference on Research and Development. doi: https://doi.org/10.1109/scored.2007.4451410

[2] Ruksana, S. K., Singh, S. K., Goswami, A. K., Sinha, N. (2018). Recent Challenges for Power Quality Impacts on Grid Integrated Wind Energy System: A Review. 2018 Second International Conference on Intelligent Computing and Control Systems (ICICCS). doi: https://doi.org/10.1109/iccons.2018.8662990

[3] Thapar, A., Saha, T. K., Zhao Yang Dong. (2004). Investigation of power quality categorisation and simulating its impact on sensitive electronic equipment. IEEE Power Engineering Society General Meeting, 2004. doi: https://doi.org/10.1109/pes.2004.1372855

[4] Jana, J., Saha, H., Das Bhattacharya, K. (2017). A review of inverter topologies for single-phase grid-connected photovoltaic systems. Renewable and Sustainable Energy Reviews, 72, 1256–1270. doi: https://doi.org/10.1016/j.rser.2016.10.049

[5] Goh, H. S., Armstrong, M., Zahawi, B. (2009). The effect of grid operating conditions on the current controller performance of grid connected photovoltaic inverters. 2009 13th European Conference on Power Electronics and Applications, 1–8. Available at: https://ieeexplore.ieee.org/document/5279106

[6] Liang, X. (2017). Emerging Power Quality Challenges Due to Integration of Renewable Energy Sources. IEEE Transactions on Industry Applications, 53 (2), 855–866. doi: https://doi.org/10.1109/tia.2016.2626253

[7] Bollen, M., Zhong, J., Zavoda, F. et. al. (2010). Power quality aspects of smart grids. RE&PQJ, 1 (8), 1061–1066. doi: https://doi.org/10.24084/repqj08.583

[8] Amaripadath, D., Roche, R., Joseph-Auguste, L., Istrate, D., Fortune, D., Braun, J. P., Gao, F. (2017). Power quality disturbances on smart grids: Overview and grid measurement configurations. 2017 52nd International Universities Power Engineering Conference (UPEC). doi: https://doi.org/10.1109/upec.2017.8231975

[9] Bollen, M. H. J., Das, R., Djokic, S., Ciufo, P., Meyer, J., Ronnberg, S. K., Zavodam, F. (2017). Power Quality Concerns in Implementing Smart Distribution-Grid Applications. IEEE Transactions on Smart Grid, 8 (1), 391–399. doi: https://doi.org/10.1109/tsg.2016.2596788

[10] Granados-Lieberman, D., Romero-Troncoso, R. J., Osornio-Rios, R. A., Garcia-Perez, A., Cabal-Yepez, E. (2011). Techniques and methodologies for power quality analysis and disturbances classification in power systems: a review. IET Generation, Transmission & Distribution, 5 (4), 519. doi: https://doi.org/10.1049/iet-gtd.2010.0466

[11] Bollen, M. H. J. (2003). What is power quality? Electric Power Systems Research, 66 (1), 5–14. doi: https://doi.org/10.1016/s0378-7796(03)00067-1

[12] Saini, M. K., Kapoor, R. (2012). Classification of power quality events – A review. International Journal of Electrical Power & Energy Systems, 43 (1), 11–19. doi: https://doi.org/10.1016/j.ijepes.2012.04.045

[13] Understanding power quality problems: voltage sags and interruptions (2000). Choice Reviews Online, 37 (08), 37-4522–37-4522. doi: https://doi.org/10.5860/choice.37-4522

[14] Emanuel, A. E. (2004). Summary of IEEE Standard 1459: Definitions for the Measurement of Electric Power Quantities Under Sinusoidal, Nonsinusoidal, Balanced, or Unbalanced Conditions. IEEE Transactions on Industry Applications, 40 (3), 869–876. doi: https://doi.org/10.1109/tia.2004.827452

[15] Deokar, S. A., Waghmare, L. M. (2014). Integrated DWT–FFT approach for detection and classification of power quality disturbances. International Journal of Electrical Power & Energy Systems, 61, 594–605. doi: https://doi.org/10.1016/j.ijepes.2014.04.015

[16] Decanini, J. G. M. S., Tonelli-Neto, M. S., Malange, F. C. V., Minussi, C. R. (2011). Detection and classification of voltage disturbances using a Fuzzy-ARTMAP-wavelet network. Electric Power Systems Research, 81 (12), 2057–2065. doi: https://doi.org/10.1016/j.epsr.2011.07.018

[17] Naderian, S., Salemnia, A. (2016). An implementation of type-2 fuzzy kernel based support vector machine algorithm for power quality events classification. International Transactions on Electrical Energy Systems, 27 (5), e2303. doi: https://doi.org/10.1002/etep.2303

[18] Lazzaretti, A. E., Ferreira, V. H., Neto, H. V. (2016). New Trends in Power Quality Event Analysis: Novelty Detection and Unsupervised Classification. Journal of Control, Automation and Electrical Systems, 27 (6), 718–727. doi: https://doi.org/10.1007/s40313-016-0265-z

[19] Borges, F. A. S., Fernandes, R. A. S., Silva, I. N., Silva, C. B. S. (2016). Feature Extraction and Power Quality Disturbances Classification Using Smart Meters Signals. IEEE Transactions on Industrial Informatics, 12 (2), 824–833. doi: https://doi.org/10.1109/tii.2015.2486379

[20] Shukla, S., Mishra, S., Singh, B. (2009). Empirical-Mode Decomposition With Hilbert Transform for Power-Quality Assessment. IEEE Transactions on Power Delivery, 24 (4), 2159–2165. doi: https://doi.org/10.1109/tpwrd.2009.2028792

[21] Gu, I. Y.-H., Styvaktakis, E. (2003). Bridge the gap: signal processing for power quality applications. Electric Power Systems Research, 66 (1), 83–96. doi: https://doi.org/10.1016/s0378-7796(03)00074-9

[22] Huang, N. E., Shen, Z., Long, S. R., Wu, M. C., Shih, H. H., Zheng, Q. et. al. (1998). The empirical mode decomposition and the Hilbert spectrum for nonlinear and non-stationary time series analysis. Proceedings of the Royal Society of London. Series A: Mathematical, Physical and Engineering Sciences, 454 (1971), 903–995. doi: https://doi.org/10.1098/rspa.1998.0193

[23] Rofii, F., Naba, A., Dharmawan, H. A., Hunaini, F. (2020). Analysis of Electrical Power Quality Disturbances Based on Empirical Mode Decomposition and Statistical Parameters. IOP Conference Series: Materials Science and Engineering, 846 (1), 012050. doi: https://doi.org/10.1088/1757-899x/846/1/012050

[24] Chattopadhyay, S., Mitra, M., Sengupta, S. (2011). Electric Power Quality. Electric Power Quality, 5–12. doi: https://doi.org/10.1007/978-94-007-0635-4_2

[25] IEEE Recommended Practice for Monitoring Electric Power Quality. doi: https://doi.org/10.1109/ieeestd.2019.8796486

[26] IEEE Standard Definitions for the Measurement of Electric Power Quantities Under Sinusoidal, Nonsinusoidal, Balanced, or Unbalanced Conditions. doi: https://doi.org/10.1109/ieeestd.2010.5439063

[27] Igual, R., Medrano, C., Arcega, F. J., Mantescu, G. (2018). Integral mathematical model of power quality disturbances. 2018 18th International Conference on Harmonics and Quality of Power (ICHQP). doi: https://doi.org/10.1109/ichqp.2018.8378902

[28] Durak, L., Arikan, O. (2003). Short-time fourier transform: two fundamental properties and an optimal implementation. IEEE Transactions on Signal Processing, 51 (5), 1231–1242. doi: https://doi.org/10.1109/tsp.2003.810293

[29] Svozil, D., Kvasnicka, V., Pospichal, J. (1997). Introduction to multi-layer feed-forward neural networks. Chemometrics and Intelligent Laboratory Systems, 39 (1), 43–62. doi: https://doi.org/10.1016/s0169-7439(97)00061-0

[30] Kliment, T., Markovič, J., Šmigura, D., Adam, P. (2019). Diagnosis of the Accuracy of the Vehicle Scale Using Neural Network. Measurement Science Review, 19 (1), 14–19. doi: https://doi.org/10.2478/msr-2019-0003

[31] Rostami, A., Anbaz, M. A., Erfani Gahrooei, H. R., Arabloo, M., Bahadori, A. (2018). Accurate estimation of CO2 adsorption on activated carbon with multi-layer feed-forward neural network (MLFNN) algorithm. Egyptian Journal of Petroleum, 27 (1), 65–73. doi: https://doi.org/10.1016/j.ejpe.2017.01.003

[32] Kouziokas, G. N., Chatzigeorgiou, A., Perakis, K. (2018). Multilayer Feed Forward Models in Groundwater Level Forecasting Using Meteorological Data in Public Management. Water Resources Management, 32 (15), 5041–5052. doi: https://doi.org/10.1007/s11269-018-2126-y

[33] Kanirajan, P., Suresh Kumar, V. (2015). Power quality disturbance detection and classification using wavelet and RBFNN. Applied Soft Computing, 35, 470–481. doi: https://doi.org/10.1016/j.asoc.2015.05.048

[34] Adnan, J., Daud, N. G. N., Ishak, M. T., Rizman, Z. I., Rahman, M. I. A. (2018). Tansig activation function (of MLP network) for cardiac abnormality detection. AIP Conference Proceedings. doi: https://doi.org/10.1063/1.5022900

[35] Shuqing, G., Yucong, S. (2021). Traffic sign recognition based on HOG feature extraction. Journal of Measurements in Engineering, 9 (3), 142–155. doi: https://doi.org/10.21595/jme.2021.22022

[36] Olivia Florencias-Oliveros, M. J. Espinosa-Gavira, Juan-José González de la Rosa, A. Agüera-Pérez, José Carlos Palomares-Salas, J. M. Sierra-Fernández. (2017). Real-life Power Quality Sags. IEEE Dataport. doi: https://doi.org/10.21227/H2K88D

*Received date 08.09.2021*
*Accepted date 12.03.2022*
*Published date 31.03.2022*



***How to cite:*** *Rofii, F., Naba, A., Dharmawan, H. A., Hunaini, F. (2022). Development of empirical mode decomposition based neural network for power quality disturbances classification. EUREKA: Physics and Engineering, 2, 28–44. doi: https://doi.org/10.21303/2461-4262.2022.002046*